Original Article

Institution of MECHANICAL ENGINEERS
Journal of AUTOMOBILE ENGINEERING

Proc IMechE Part D:
J Automobile Engineering
1–13

DOI: 10.1177/09544070251330662
journals.sagepub.com/home/pid
Sage

Analyzing and comparing the mechanical behaviors of bio-inspired ribbed rectangular and square tubes

DucHieu Le[1], PhucThien Nguyen[2] and TrongNhan Tran[3]

Abstract

This study delves into the axial crushing behavior of bionic rectangular and square tubes, both with and without ribs, through experimental methods. The bionic structures are meticulously fabricated by integrating thin tubes, thicker ribs, and spot welding. The crashworthiness performance is evaluated for thicker square tubes without ribs and thinner square and rectangular tubes with ribs, taking into account critical factors such as ribs, sections, and spot welding. Compared to the tube without ribs (90902), which has a higher peak crushing force (PCF) of 250.94 kN and a lower crushing force ratio (CFR) of 0.30, ribbed tubes exhibit a 43.24% lower average PCF (142.42 kN), and a 58.47% higher average CFR (0.476). Ribbed square tubes outperform their rectangular counterparts in specific energy absorption (SEA), with BRST1 specimens achieving a 42.94% higher mean SEA (12.75 kJ/kg) compared to BRRT1 specimens (8.92 kJ/kg), despite the latter having a higher PCF. Consequently, the study underscores the effectiveness of incorporating thin tubes with thicker ribs and spot welding in the construction of energy absorbers.

Keywords

Energy absorption, crashworthiness, bio-inspired square and rectangular tube, ribs, axial loading

Date received: 19 December 2024; accepted: 11 March 2025

Introduction

Despite advancements in vehicle safety performance over time, collisions continue to inflict damage on passengers and property. Passive safety, which focuses on maintaining the survival space for passengers during collisions, remains a critical aspect of transportation safety. Over the past decade, extensive studies on crashworthiness performance have been conducted to enhance occupant protection during crushing events.[1] Tubular components are essential in absorbing the crushing force and mitigating harm to passengers. Consequently, research on tubular parts has garnered significant attention in recent years.

The outer shapes of tubular parts designed to dissipate crushing loads exhibit considerable variation, encompassing square,[2] rectangular,[3] circular,[4] tapered,[5] and corrugated[6] configurations. Among these, the behavior of circular tubes was initially examined by Coppa,[7] who identified deformation modes such as concertina, diamond, and Euler modes, contingent on the t/D ratio.[8] Subsequent research shifted focus to square tubes, beginning with the work of Abramowicz and Jones.[9] This line of inquiry expanded to include modified square tubes, such as multi-corner tubes,[10] multi-cell tube,[11] and tube with aluminum foam,[12] or honeycomb[13] structures. These studies demonstrated enhanced crashworthiness performance for the modified square tubes.[14] For example, Nia and Attar[15] investigated the crashworthiness of square tubes with and without stiffeners, emphasizing the impact of the number and placement of stiffeners. Their study also highlighted discrepancies in crashworthiness index values between experimental tests and simulations, attributing these differences to fabrication imperfections. Rajak et al.[16] assessed the energy absorption capacity

[1]Faculty of Transportation Engineering, School of Mechanical and Automotive Engineering, Hanoi University of Industry, Hanoi, Vietnam
[2]Faculty of Engineering and Technology, Van Hien University, Ho Chi Minh City, Vietnam
[3]Faculty of Mechanical Engineering, Industrial University of Ho Chi Minh City, Ho Chi Minh City, Vietnam

Corresponding author:
TrongNhan Tran, Faculty of Mechanical Engineering, Industrial University of Ho Chi Minh City, 12 Nguyen Van Bao, Ho Chi Minh City 700000, Vietnam.
Email: trantrongnhan@iuh.edu.vn

of both hollow and foam-filled square tubes under varying strain rates in axial quasi-static loading, finding that foam-filled square tubes exhibited superior energy absorption capacity and suggested an optimized strain rate. Overall, modified or specialized structures have demonstrated superior crashworthiness performance compared to conventional designs.[17]

In addition to examining the energy absorption capabilities of single tubes, researchers have also investigated the energy absorption characteristics of nested tubes. Sharifi et al.[18] explored the impact of tube parameters and grooves on the energy absorption performance of nested circular structures. Although the introduction of grooves reduced peak forces, it also diminished the energy absorption capacity by decreasing the material volume within the structure. A comparative study on the energy absorption features of nested circular structures was conducted by Nia and Chahardoli,[19] which underscored the effect of annealing in reducing the structure's energy absorption capacity due to decreased yield and ultimate stresses. The primary distinction between these two studies lies in the number of constituent tubes analyzed. Additionally, Haghi Kashani et al.[20] investigated the energy absorption characteristics of nested square structures, focusing on the effects of tube arrangement. Their findings revealed that the nested structure exhibited greater energy absorption compared to the sum of the energy absorbed by two individual tubes when crushed independently. This enhancement in energy absorption was attributed to the interaction between the tube walls.

The quest for structures with enhanced crashworthiness performance compared to conventional designs continues to challenge designers. Consequently, innovative crashworthy designs inspired by biological structures present promising opportunities by leveraging their unique characteristics. Drawing inspiration from the cross-section of the horsetail plant, Xiao et al.[21] proposed six configurations of bionic tubes and examined the influence of design variables on their crashworthiness performance. The results indicated that increasing the number of cells, inner tube diameter, and wall thickness significantly enhanced the specific energy absorption (SEA) of the tubes. However, it is noteworthy that the SEA decreased when the wall thickness exceeded 2 mm. These findings offer valuable insights for optimizing bionic tubes to improve crashworthiness. The vascular bundle arrangement of palm trees holds significant potential as a natural template for designing highly efficient energy dissipators. Building on this inspiration, Liu et al.[22] developed bionic multicell tubes and assessed their crashworthiness performance under quasi-static loading conditions. Their findings demonstrated a remarkable improvement in crashworthiness behavior with an increase in the tube's cell number. In the study conducted by Chen et al.,[23] bionic tubes incorporating a ribbed design were evaluated and compared to conventional circular tubes in terms of crashworthiness features. Experimental results revealed that the bionic tubes with ribs exhibited a lower peak load while achieving higher specific energy absorption compared to their conventional counterparts under the same loading conditions. Tarafdar et al.[24] introduced a novel design for energy-absorbing systems that emulates the microstructure of bamboo. Their study analyzed the mechanical behavior of the structure under axial loading, highlighting that the energy absorption is influenced by the failure mechanism, which can be categorized into two sub-modes: I and II.

Previous studies have examined the impact of adding ribs on the energy absorption capabilities of tubes. However, this study aims to investigate the crashworthiness performance of thin tubes, both with and without thicker ribs, drawing inspiration from biological concepts. The inclusion of thicker ribs is intended to enhance the crashworthiness of the thin tubes. A comprehensive comparison between square and rectangular tubes, with and without ribs, was conducted to assess the influence of ribs, sectional design, and spot welding on their energy absorption characteristics. Consequently, this study focuses on experimentally investigating the crashworthiness features of bionic tubes and analyzing their behavior.

Specimens and test setup

The rapidly expanding field of bio-inspired design leverages insights from nature to develop superior designs compared to conventional ones. The prismatic layer microstructure of the Pinna, illustrated in Figure 1(a), where the upper walls connect to the lower tube walls, and the cross-section of the lower tubes may not be hexagonal, serves as inspiration for a novel tube design aimed at enhancing existing tubes. This proposed design involves integrating four thicker ribs into a single tube with a new cross-section. In this study, we have selected rectangular and square sections, which literature validates as effective anti-crushing cross-sections. The reference specimen for comparison is a single square tube measuring $90 \times 90 \times 2$ mm without ribs, as shown in Figure 1(b). We then investigate the mechanical behaviors of the reference (90902) specimen, as well as the bio-inspired ribbed rectangular (BRRT) and square (BRST) tubes depicted in Figure 1(c).

To construct the ribbed specimens, tubes and ribs were cut separately from 6 m-long CT3 mild steel[25] tube and strip, respectively. Subsequently, each individual tube was slit to precise dimensions before being assembled using spot welding techniques (refer to Figure 1(c)). The rectangular or square tubes have a depth and width denoted as a and b, respectively, while the rib width is denoted as b_1. The tube wall and rib thicknesses are labeled as t and t_1, respectively, and the height of both the tube and rib measures 200 mm. The parameters of all specimens are presented in Table 1.

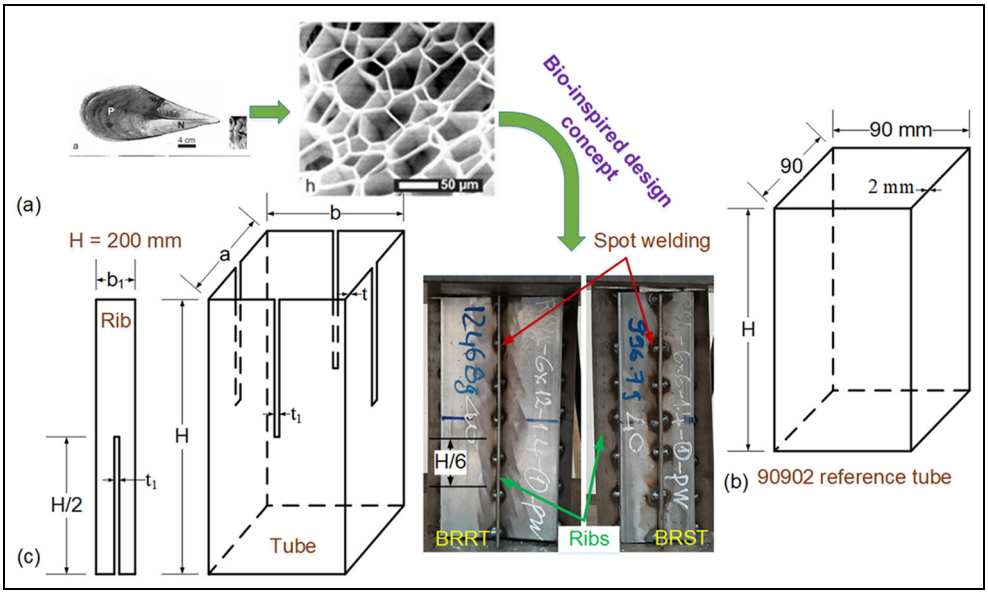

Figure 1. (a) Bio-inspired design concept,[26] (b) bio-inspired ribbed rectangular (BRRT) and square (BRST) tubes, and (c) reference specimen.

Table 1. Tube parameters with features.

Tube	Tube			Rib		Height (mm)	m (kg)	Features
	a (mm)	*b* (mm)	*t* (mm)	*b*1 (mm)	*t*1 (mm)			
90902	90	90	2	–	–	200	1.079	No ribs
BRRT1-1	50	100	1.31	40	1.4		1.099	*Spot welding * Four ribs *Rectangular section
BRRT1-2							1.116	
BRRT1-3							1.113	
BRRT2-1	60	120					1.247	
BRRT2-2							1.245	
BRRT2-3							1.236	
BRST1-1	60	60					0.997	* Spot welding
BRST1-2							1.000	*Four ribs
BRST2-1	70	70					1.130	*Square section
BRST2-2							1.129	
BRST2-3							1.128	
BRST3-1	90	90					1.261	
BRST3-2							1.256	
BRST3-3							1.255	

As one of the recognized methods for investigating the behavior of energy-absorbing elements,[27] the bio-inspired ribbed rectangular or square tubes were subjected to quasi-static axial testing using a testing machine with a capacity of 500 kN, as depicted in Figure 2. The specimen was positioned on the machine's lower disc without any constraints. To prevent potential damage to the machine, the final crushing displacement (z_{final}) of the test was set at 165 mm. A loading rate of 5 mm/min^1 was employed, and the crushing process was captured using a camera. Force-displacement curves were directly recorded to determine the crashworthiness parameters. Figure 3 illustrates a typical force response obtained from the experimental testing.

The mechanical behavior of the structure is influenced by several key parameters associated with the crushing process, namely peak crushing force (PCF), energy absorption (EA),[28] specific energy absorption (SEA),[29] mean crushing force (MCF), and crushing force ratio (CFR). Table 2 provides the expressions used to estimate these key parameters. PCF is directly obtained from the force response and should be sufficiently small to initiate the deformation of the tube. EA represents the total energy absorbed by the tube during the crushing event. SEA is calculated by dividing EA by

Table 2. Expression of crashworthiness indexes.

Crushing key parameter	Expression
Energy absorption (EA)	$EA = \int_0^{z_{final}} F(x)dx$
Specific energy absorption (SEA)	$SEA = \frac{EA}{m}$
Mean crushing force (MCF)	$MCF = \frac{EA}{z_{final}}$
Crushing force ratio (CFR)	$CFR = \frac{MCF}{PCF}$

Here, m is the tube's mass and z_{final} is the final crushing displacement.

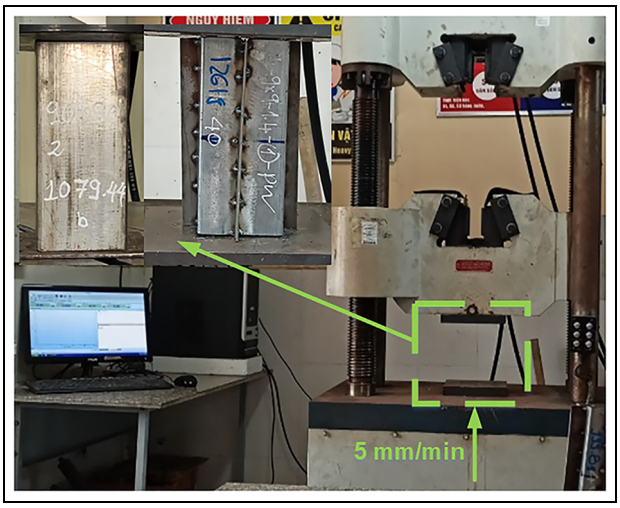

Figure 2. Experimental testing.

the mass of the tube. MCF refers to the average force experienced during the collapse process and is estimated by dividing the energy absorption by the final crushing displacement (z_{final}). Lastly, CFR is expressed as a percentage and is determined by the ratio of MCF to PCF.

Investigation of compression test of all specimens

When a ductile metal tube is subjected to an axial load, it undergoes gradual deformation, with its typical force response following the pattern illustrated in Figure 3. The crushing process can be divided into three distinct stages: pre-crush, post-crush, and densification. In the initial pre-crush stage, the tube behaves elastically until the crushing force reaches its peak. However, as instability develops, the force drops sharply until the formation of the first lobe wall, with the peak force being dependent on the tube's anti-crushing capacity. During the post-crush stage, the mean crushing force fluctuates, exhibiting peaks and valleys directly linked to the shape and crumpling at various wrinkling levels. Eventually, densification occurs due to the self-contact

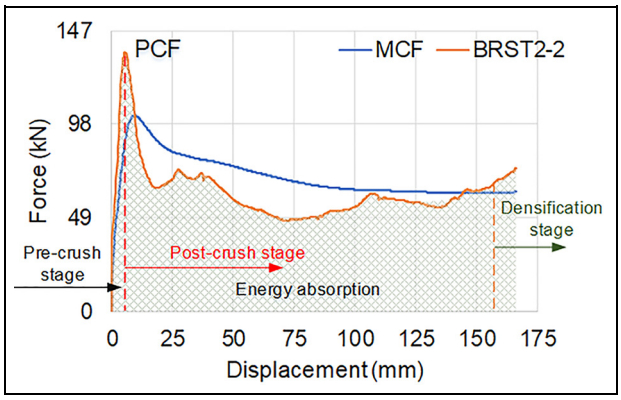

Figure 3. Typical force response of energy absorbing tube.

of lobes, leading to the overlap of completed lobes and a significant increase in load.

This section presents a study of the behavior, force, and energy absorption responses of all specimens. To ensure the reliability of the results, three experiments were conducted for each BRRT1, BRRT2, BRST2, and BRST3 architecture, with BRST1 having two tests and the reference tube having one.

90902 reference specimen

The crushing behavior of the reference specimen serves as the basis for comparison with other tubes. Figure 4(a) displays snapshots of the collapsing process of the 90902 specimen under axial loading. The initial buckling lines of the first lobe form near the top end of the tube, followed by successive buckling lines that create the second lobe. As the collapsing process continues, the first lobe stacks onto the second one. This deformation pattern promotes a stable collapse of the reference tube under axial loading. However, due to the large cross-section and limited height of the tube, the lobes are not fully deformed at both ends.

The force response of the tube, shown in Figure 4(b), demonstrates a stable energy-absorbing process during the collapse under axial loading (Figure 4(c)). Nonetheless, there is a significant difference of 90.83 kN between the first and second peak forces, reflecting the transition from the elastic response to plastic deformation. The compressive force, defined as the axial force applied to deform the tube, fluctuates considerably during plastic deformation in the post-crush stage, ranging from 46.61 to 155.23 kN. These values correspond to the minimum and maximum force observed in the force response presented in Figure 4(b). Such high fluctuation in compressive force is not desirable for an anti-crushing element.

Bio-inspired ribbed rectangular tubes (BRRT1)

The crushing history, force response, and energy absorption response of all three BRRT1 specimens are

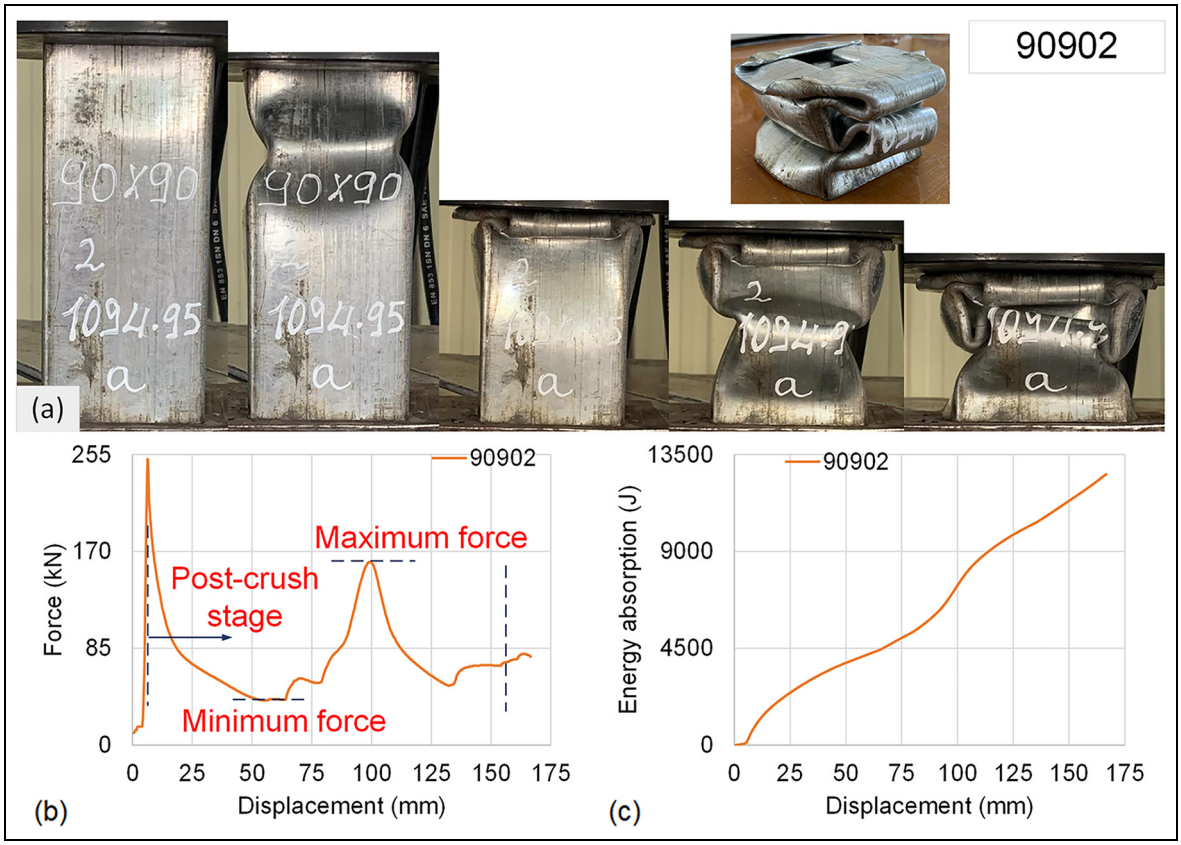

Figure 4. 90902. (a) Crushing history and its final shape, (b) force, and (c) EA responses.

exhibited in Figure 5. In Figure 5(a), the crushing history of the BRRT1 specimens reveals varying pre-crush behaviors, with the first bending lines in the tube walls developing randomly at the bottom, top, or middle of the tube. The post-crush stages of these specimens also differ to some extent. Such variations in collapsing behaviors are expected, as outcomes vary from specimen to specimen due to sensitivity to imperfections in geometry and material, despite careful fabrication. For all three specimens, namely BRRT1-1, BRRT1-2, and BRRT1-3, their crushing histories differ from each other, and the wavelength of the lobes in the tube is smaller than that in the ribs.

The ribs of BRRT1-1 and BRRT1-3 formed more complete lobes compared to those of BRRT1-2, while the number of lobes in the ribs of BRRT1-1 and BRRT1-2 are the largest and smallest, respectively. Greater rib thickness required higher compressive forces to deform them; hence, the lobes were easier to form in the tube than in the ribs. The differing number and wavelength of lobes in the tube and ribs resulted in weld cracking, shown in red ellipses, causing the tube and ribs of each specimen to bear the load independently. Such crushing histories may be attributed to weld quality and the difference in thickness between the ribs and tube, leading to a decrease in crushing strength and energy dissipation capacity.

The crushing histories of these specimens are clearly reflected in the force and energy absorption responses shown in Figure 5(b) and (c). In Figure 5(b), the PCF of BRRT1-2 and BRRT1-3 are larger than that of BRRT1-1. However, the force history of BRRT1-2 is more stable and smoother in the post-crush stage, despite the higher force levels of BRRT1-1 and BRRT1-3. This is because the higher force levels of BRRT1-1 and BRRT1-3 lead to the formation of more plastic hinges, which in turn requires a lower crushing force level for deformation. Consequently, this results in lower energy absorption (EA) in the later stages of compression for BRRT1-1 and BRRT1-3, as shown in Figure 5(c).

Bio-inspired ribbed rectangular tubes (BRRT2)

The deformations of the three specimens in the BRRT2 group are illustrated in Figure 6(a). Despite meticulous prototyping, variations were observed in their collapsing processes. The collapse of BRRT2-2 initiated from the bottom end, differing from BRRT2-1 and BRRT2-3, which began collapsing from the top end. In the BRRT2 group, the formation of the first lobes in the ribs and tube occurred simultaneously during the initial half of the compression, with no weld fractures observed, indicating that the crushing load remained

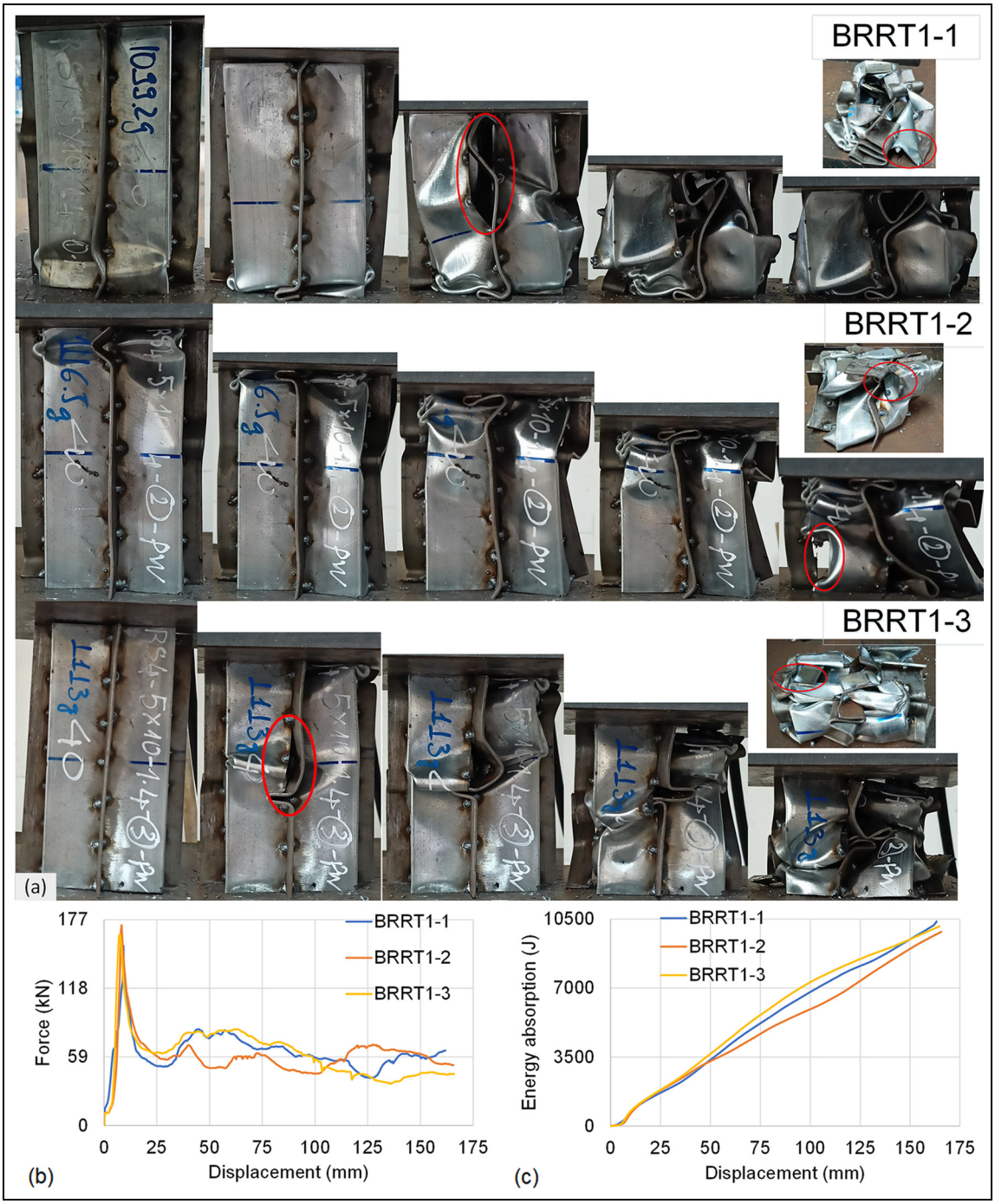

Figure 5. BRRT1. (a) Crushing history and their final shapes, (b) force response, and (c) EA response.

below the weld strength. However, in the later stages of the crushing process, the tube and ribs of the BRRT2 specimens did not form complete lobes. Additionally, variations in the lobe shapes between the tube and ribs at this stage resulted from heterogeneous deformation between the two components, leading to weld fractures and a decrease in crushing strength. The fractures in the welds and bending in the tube primarily occurred at the slots in the tube.

Figure 6(b) and (c) depict the force and energy absorption histories of the specimens, respectively, corresponding to their crushing behaviors. It is evident that there is a significant decrease in anti-crushing strength, as indicated by the drop in crushing force towards the end of compression. BRRT2-3 exhibits a delayed attainment of its first peak force compared to the other two specimens, and its crushing force level in the later stages of deformation is higher. Consequently,

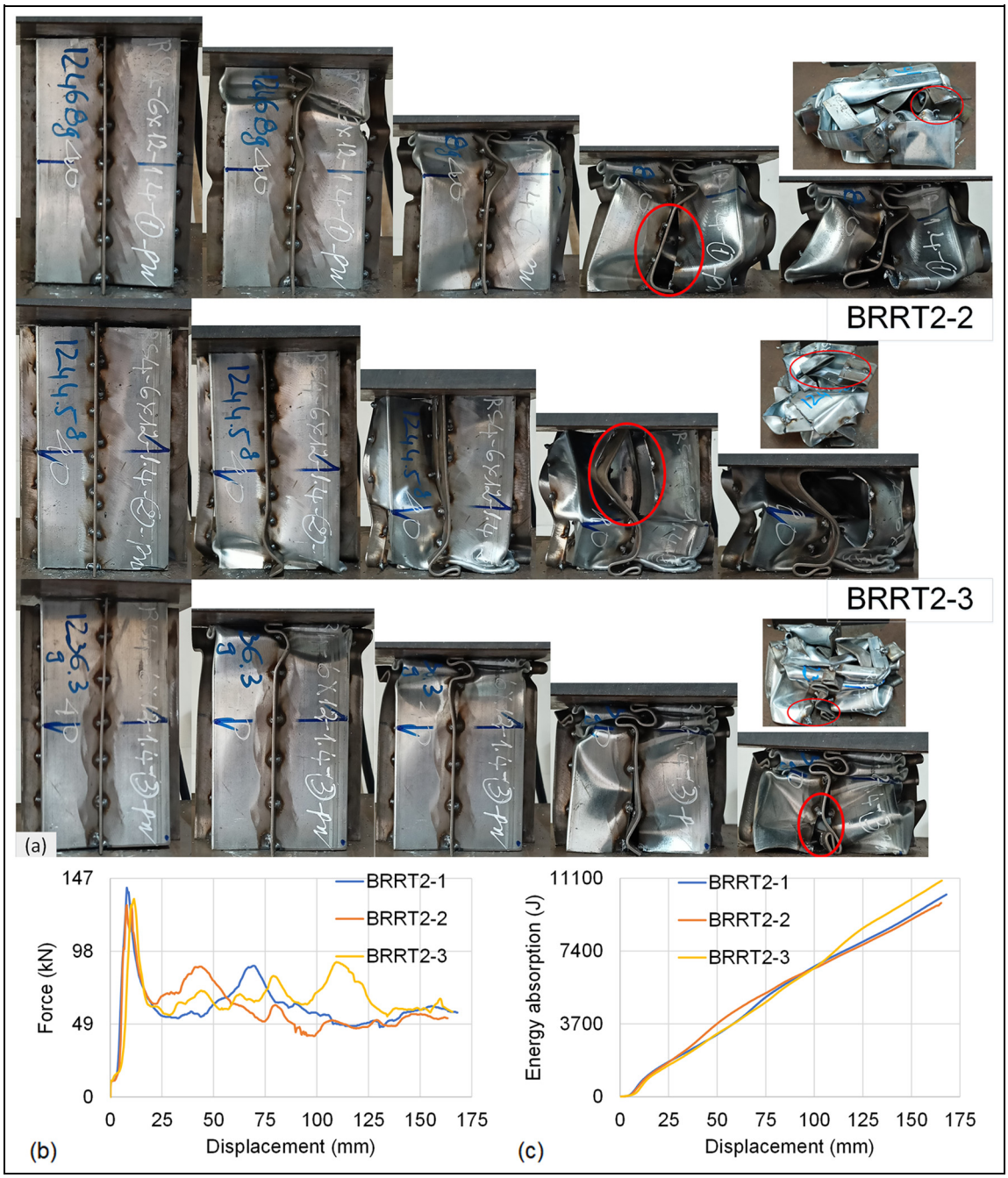

Figure 6. BRRT2. (a) Crushing history and their final shapes, (b) force, and (c) EA responses.

BRRT2-3 demonstrates greater energy absorption in this stage (Figure 6(c)).

Bio-inspired ribbed square tubes (BRST1)

The failure mechanisms and final shapes of the BRST1 specimens are illustrated in Figure 7(a). During the collapsing process, both specimens began to wrinkle from the upper end, forming the first lobe, followed by successive lobes stacking on top of the initial one. Their failure mechanisms are similar, exhibiting good progressive collapse in the early stage and buckling collapse in the later stage of compression. Buckling primarily occurs in the slotted part, reducing its energy absorption capacity. Progressive deformation occurred in the ribs of BRST1-2 but not in those of BRST1-1, although fractures were present in the welds of both specimens. The progressive deformation in the ribs enhanced the energy absorption capacity of BRST1-2. The minor differences in failure mechanisms between these two specimens are linked to weld quality and the interaction between lobe formation in the tube and ribs.

Figure 7(b) shows comparable force-displacement curves for the two BRST1 specimens due to the similarity in their failure mechanisms, as shown in Figure 7(a). The first peak forces of these two specimens occur at

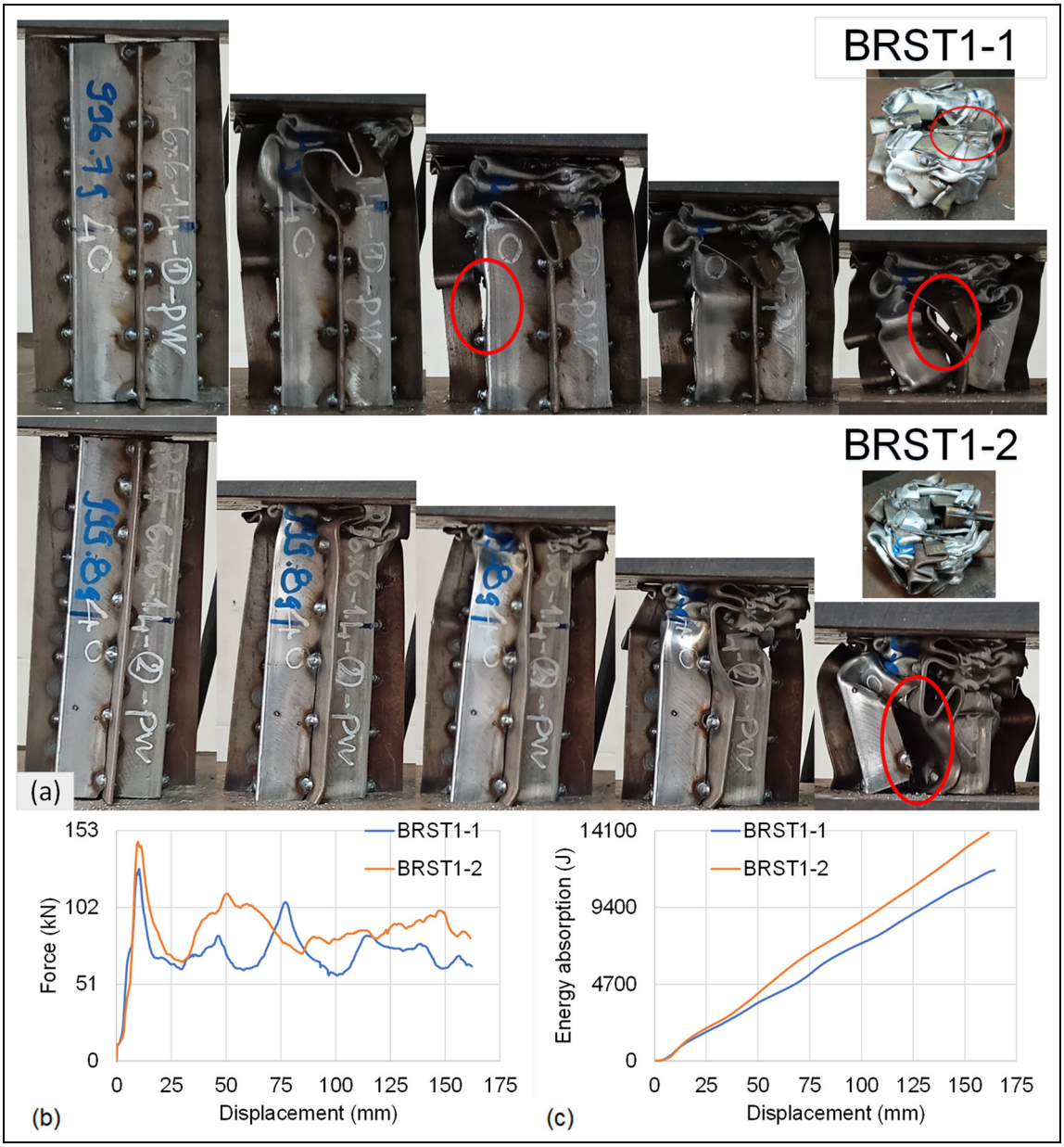

Figure 7. BRST1. (a) Crushing history and their final shapes, (b) force response, and (c) EA response.

almost the same crushing displacement; however, BRST1-2 exhibits a higher force level than BRST1-1 due to its greater anti-crushing resistance, resulting in a greater capacity to absorb collapsing energy (Figure 7(c)).

Bio-inspired ribbed square tubes (BRST2)

Figure 8(a) presents the failure mechanisms and final deformation shapes of the BRST2 specimens, which exhibit distinct differences among them. In all three specimens, the first plastic hinges were observed near the upper ends, and the collapses progressed from top to bottom. Similar to the BRST1 specimens, fractures in the welds resulted in buckling in the slotted part, thereby reducing the structure's energy absorption capability. Although all three specimens experienced weld fractures, BRST2-1 demonstrated better progressive deformation compared to the other two specimens. Progressive deformation was observed in the ribs of BRST2-1, enhancing its energy absorption capacity. BRST2-2 exhibited torsional deformation, an undesired mode under axial load, due to a fabrication imperfection, thereby reducing its energy absorption capacity. While progressive deformation occurred in the ribs of BRST2-3 during the early stage, fractures in the welds hindered this mode in the later stage of the collapse process, resulting in decreased anti-crushing capacity and energy absorption.

The effect of failure mechanisms on force and energy absorption responses of these specimens is shown in Figure 8(b) and (c), indicating larger force and energy absorption levels for BRST2-1 compared to BRST2-2

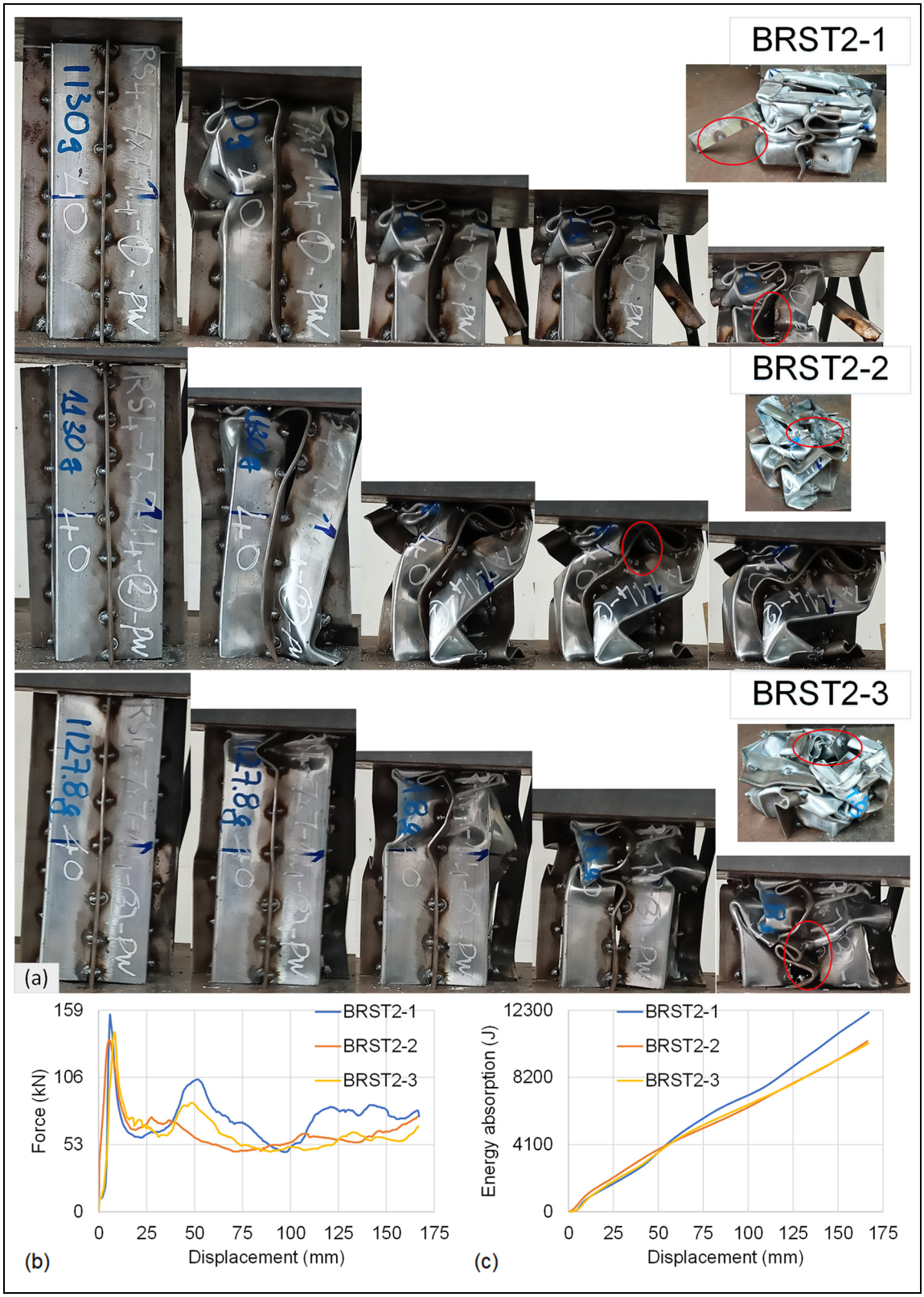

Figure 8. BRST2. (a) Crushing history and their final shapes, (b) force response, and (c) EA response.

and BRST2-3. Although in the early stage, BRST2-3's PCF appears later and greater than that of BRST2-2, their force levels are approximately equal in the subsequent stage of the crushing process, resulting in equivalent energy absorption levels, as depicted in Figure 8(c).

Bio-inspired ribbed square tubes (BRST3)

The collapsing histories, as well as the force and energy absorption behaviors of the BRST3 specimens, are presented in Figure 9. The first creasing lines developed in

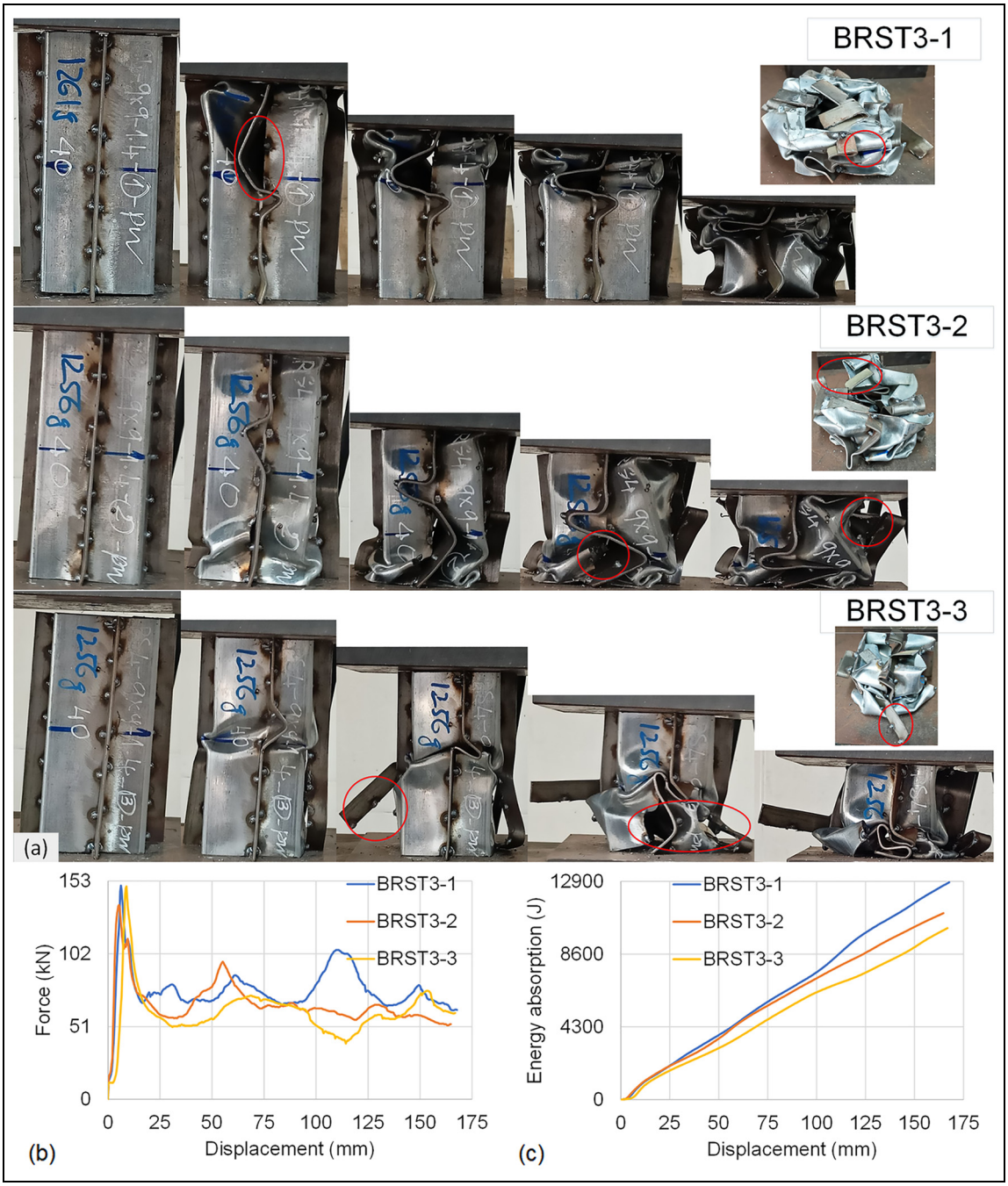

Figure 9. BRST3. (a) Crushing history and their final shapes, (b) force, and (c) EA responses.

different locations for each specimen: near the top end of BRST3-1, near the bottom end of BRST3-2, and in the middle of BRST3-3 (Figure 9(a)). The deformation continued until the crushing process concluded. Initially, progressive deformation occurred in the tube and ribs of the BRST3-1 and BRST3-2 specimens. However, these specimens later crumpled due to the fracture of the welds between the tube and ribs. The collapse of BRST3-3 occurred at the position with the weakest anti-collapsing resistance, leading to the fracture of the welds and the buckling of the specimen under axial loading. The fractures in the welds of BRST3-3 and BRST3-1 were, respectively, the largest and the smallest, which determined their anti-crushing and energy absorption capacities.

The energy absorption capacity of the structure primarily depends on the post-crush stage of compression. Figure 9(b) demonstrates that the PCF and force fluctuation of BRST3-1 are larger than those of BRST3-2 and BRST3-3, leading to greater energy absorption in the displacement range of 25 mm to 165 mm, as shown in Figure 9(c).

Table 3. Main indexes for all specimens.

Tube	PCF (kN)	MCF (kN)	CFR	SEA (kJ/kg)	EA (kJ)	m (kg)
90902	250.94	75.424	0.30	11.085	12.137	1.0794
BRRT1-1	154.49	62.94	0.51	9.22	10.13	1.099
BRRT1-2	172.25	59.70	0.35	8.61	9.61	1.116
BRRT1-3	164.27	61.92	0.38	8.95	9.96	1.113
BRRT1 (mean)	163.67	61.52	0.41	8.92	9.90	1.109
BRRT2-1	140.73	61.25	0.44	7.90	9.86	1.247
BRRT2-2	127.26	59.61	0.47	7.71	9.59	1.245
BRRT2-3	133.25	66.46	0.50	8.65	10.70	1.236
BRRT2 (mean)	133.75	62.44	0.47	8.09	10.05	1.242
BRST1-1	124.98	71.64	0.57	11.57	11.53	0.997
BRST1-2	145.53	86.59	0.59	13.94	13.93	1.000
BRST1 (mean)	135.26	79.11	0.58	12.75	12.73	0.998
BRST2-1	155.66	72.67	0.47	10.35	11.69	1.130
BRST2-2	135.72	62.29	0.46	8.88	10.02	1.129
BRST2-3	141.84	61.62	0.43	8.79	9.91	1.128
BRST2 (mean)	144.40	65.52	0.45	9.34	10.54	1.129
BRST3-1	149.77	77.08	0.51	9.84	12.40	1.261
BRST3-2	136.17	67.23	0.49	8.61	10.82	1.256
BRST3-3	149.18	60.74	0.41	7.79	9.77	1.255
BRST3 (mean)	145.04	68.35	0.47	8.75	11.00	1.257

Factors affecting the collapse characteristics

An investigation should be conducted to examine the effect of various factors involved in specimen formation, including ribs, geometrical parameters, cross-section, and spot welds, as these factors significantly influence the crushing behavior and key indexes related to crashworthiness. Table 3 presents a comparison of the 90902 specimen with BRRT1, BRRT2, BRST2, BRST3, and BTST1 specimens in terms of weight. The 90902 specimen is found to be 2.77% lighter than BRRT1, 15.1% lighter than BRRT2, 4.58% lighter than BRST2, and 16.48% lighter than BRST3. However, it is 7.51% heavier than BTST1. Notably, there are variations in the values of the key indexes provided in Table 3. These differences can be attributed to the fabrication process and material heterogeneity encountered during testing, but they remain within acceptable tolerances.

In general, an increase in PCF often corresponds to a higher energy absorption capacity,[30] and this observation holds true for the 90902 specimen, which does not have ribs, as well as the BRST1 specimen. However, it is important to note that the quality of spot welds significantly influences the crashworthiness indexes. For instance, in the case of BRRT1, despite BRRT1-2 having a higher PCF, its energy absorption is significantly lower than that of BRRT1-1. This indicates that BRRT1-2 exhibits a greater initial anti-crushing resistance of the spot welds but a weaker anti-crushing resistance in the later stages of crushing compared to BRRT1-1. The decreased anti-crushing resistance of spot welds during the later compression stage leads to more frequent fractures in these welds for BRRT1-2 (see Figure 5(a)). Similar results can be observed for specimens in the BRRT2, BRST2, and BRST3 groups.

Compared to the 90902 specimen, the average PCF of the specimens with ribs – namely BRRT1, BRRT2, BRST1, BRST2, and BRST3 – is ~43.24% smaller. However, their average CFR is 58.47% larger. This result demonstrates that the spot-welding method significantly reduces the PCF of ribbed specimens compared to single tubes with larger geometries and thicknesses. Consequently, this reduction in PCF helps minimize potential damage to occupants during a crushing event. Although the average MCF, SEA, and EA of the 90902 specimen are greater than those of BRRT1, BRRT2, BRST2, and BRST3 by 14.53%, 20.48%, and 14.53%, respectively, they are smaller than those of BRST1 by 4.89%, 15.03%, and 4.89%, respectively. This is due to the simultaneous deformation of the tube and ribs in BRST1, which involves a larger amount of material in plastic deformation.[31] Despite the better MCF, EA, and SEA performance, the 90902 specimen exhibits the largest PCF and the smallest CFR, which are undesirable as these two indexes negatively impact crashworthiness.

In crashworthiness design, an energy-absorbing structure typically requires a large SEA and a sufficiently small PCF to deform the structure.[5] The BRRT1 and BRRT2 specimens demonstrate similar energy absorption and comparable SEA and PCF values, indicating that the effect of geometrical parameters in these specimens is comparable. Similar conclusions can be drawn for the BRST1, BRST2, and BRST3 specimens. However, it is evident that ribbed square tubes with small sections and thicknesses are more favorable

for energy-absorbing structures. The effect of geometrical parameters, such as width and depth, on crushing force and energy absorption is more pronounced than their effect on SEA.

Overall, Table 3 illustrates that as the ribbed square tube becomes larger, the PCF, MCF, and EA increase, while the SEA decreases, except in the case of BRST1. For ribbed rectangular tubes, larger cross-sections result in smaller PCF and SEA values, indicating that specimens with larger cross-sections are more prone to deformation. The mass of the specimen plays a significant role in its energy absorption efficiency. Additionally, Table 3 suggests that ribbed rectangular tubes exhibit greater anti-crushing characteristics but lower energy absorption efficiency compared to ribbed square tubes.

Conclusion

This study presents an experimental investigation of tubes, both with and without ribs, under axial quasi-static loading conditions. The results obtained are compared to analyze the impact of ribs, geometrical parameters, cross-section, and fabrication on crashworthiness performance. The following conclusions can be drawn:

1. Tubes without ribs (90902) have a higher PCF of 250.94 kN compared to ribbed tubes. In contrast, the average PCF for ribbed tubes (BRRT1, BRRT2, BRST1, BRST2, and BRST3) is ~43.24% lower, with a mean value of around 142.42 kN. This reduction demonstrates the effectiveness of rib integration in lowering initial peak force.
2. The CFR is notably lower in the tube without ribs (90902) at 0.30. Conversely, ribbed tubes demonstrate a considerably higher average CFR of 0.476, representing a 58.47% increase over the reference tube. A lower CFR indicates reduced effectiveness in energy absorption.
3. Ribbed square tubes surpass their rectangular counterparts in SEA. Notably, BRST1 specimens achieve a 42.94% higher mean SEA (12.75 kJ/kg) than BRRT1 specimens (8.92 kJ/kg), despite the latter's higher PCF.
4. For ribbed rectangular tubes, increasing the cross-section leads to decreased PCF and SEA, making them easier to deform. In the case of ribbed square tubes, increasing the cross-section results in decreased SEA.
5. The spot weld method reduces the PCF and mass of the specimen, thereby improving its crashworthiness performance. In comparison to thick tubes without ribs, thinner square tubes with thick ribs offer advantages in crashworthy design.

Future research could extend this work by comparing the crashworthiness of ribbed tubes fabricated using spot welding and fillet welds, as well as by optimizing the ribbed tubes' parameters to improve energy absorption.

Acknowledgements

The author would like to thank the Industrial University of Ho Chi Minh City (Project No. 23.1CK01), Vietnam, for supporting this work.

Declaration of conflicting interests

The author(s) declared no potential conflicts of interest with respect to the research, authorship, and/or publication of this article.

ORCID iD

TrongNhan Tran https://orcid.org/0000-0003-4148-6214

References

1. Tarafdar A, Liaghat G, Ahmadi H, et al. Quasi-static and low-velocity impact behavior of the bio-inspired hybrid Al/GFRP sandwich tube with hierarchical core: experimental and numerical investigation. *Compos Struct* 2021; 276: 114567.
2. Ha NS, Pham TM, Hao H, et al. Energy absorption characteristics of bio-inspired hierarchical multi-cell square tubes under axial crushing. *Int J Mech Sci* 2021; 201: 106464.
3. Kazi M-K, Eljack F and Mahdi E. Design of composite rectangular tubes for optimum crashworthiness performance via experimental and ANN techniques. *Compos Struct* 2022; 279: 114858.
4. Pratiknyo YB, Setiawan R and Wayan Suweca I. Experimental and theoretical investigation of combined expansion tube-axial splitting as impact energy absorbers. *Int J Struct Stab Dyn* 2019; 20(2): 2050021.
5. Hou S, Han X, Sun G, et al. Multiobjective optimization for tapered circular tubes. *Thin-Walled Struct* 2011; 49(7): 855–863.
6. Deng X, Qin S and Huang J. Energy absorption characteristics of axially varying thickness lateral corrugated tubes under axial impact loading. *Thin-Walled Struct* 2021; 163: 107721.
7. Coppa AP. On the mechanism of buckling of circular cylindrical shells under longitudinal impact. TIS report R60SD494, 1966. Boston, MA: General Electric Co.
8. Andrews KRF, England GL and Ghani E. Classification of the axial collapse of cylindrical tubes under quasi-static loading. *Int J Mech Sci* 1983; 25(9): 687–696.
9. Abramowicz W and Jones N. Dynamic axial crushing of square tubes. *Int J Impact Eng* 1984; 2(2): 179–208.
10. Liu S, Tong Z, Tang Z, et al. Bionic design modification of non-convex multi-corner thin-walled columns for improving energy absorption through adding bulkheads. *Thin-Walled Struct* 2015; 88: 70–81.

11. Abdullahi HS and Gao S. A novel multi-cell square tubal structure based on Voronoi tessellation for enhanced crashworthiness. *Thin-Walled Struct* 2020; 150: 106690.
12. Huo RY, Han D, Zhang Y, et al. Mechanical properties of auxetic circular and square tubes filled with aluminum foam. *Eng Struct* 2023; 281: 115732.
13. Gao Y and Huang H. Energy absorption characteristics and functional gradient optimization of a hybrid honeycomb. *Int J Struct Stab Dyn* 2022; 22(11): 2250117.
14. Günaydın K, Gülcan O and Türkmen HS. Experimental and numerical crushing performance of crash boxes filled with re-entrant and anti-tetrachiral auxetic structures. *Int J Crashworthiness* 2022; 25: 1–15.
15. Alavi Nia A and Akhavan Attar A. The effect of different layouts in internal and external stiffeners on the energy absorption of thin-walled structures with square sections. *Arch Civ Mech Eng* 2017; 17(4): 997–1010.
16. Rajak DK, Kumaraswamidhas LA and Das S. Investigation of mild steel thin-wall tubes in unfilled and foam-filled triangle, square, and hexagonal cross sections under compression load. *J Mat Eng Perform* 2018; 27(4): 1936–1944.
17. Ochelski S and Gotowicki P. Experimental assessment of energy absorption capability of carbon-epoxy and glass-epoxy composites. *Compos Struct* 2009; 87(3): 215–224.
18. Sharifi S, Shakeri M, Fakhari HE, et al. Experimental investigation of bitubal circular energy absorbers under quasi-static axial load. *Thin-Walled Struct* 2015; 89(supplement C): 42–53.
19. Nia AA and Chahardoli S. Mechanical behavior of nested multi-tubular structures under quasi-static axial load. *Thin-Walled Struct* 2016; 106(supplement C): 376–389.
20. Haghi Kashani M, Shahsavari Alavijeh H, Akbarshahi H, et al. Bitubular square tubes with different arrangements under quasi-static axial compression loading. *Mater Des* 2013; 51: 1095–1103.
21. Xiao Y, Yin H, Fang H, et al. Crashworthiness design of horsetail-bionic thin-walled structures under axial dynamic loading. *Int J Mech Mater Des* 2016; 12(4): 563–576.
22. Liu Q, Ma J, He Z, et al. Energy absorption of bio-inspired multi-cell CFRP and aluminum square tubes. *Compos B Eng* 2017; 121: 134–144.
23. Chen BC, Zou M, Liu GM, et al. Experimental study on energy absorption of bionic tubes inspired by bamboo structures under axial crushing. *Int J Impact Eng* 2018; 115: 48–57.
24. Tarafdar A, Razmkhah O, Ahmadi H, et al. Effect of layering layout on the energy absorbance of bamboo-inspired tubular composites. *J Reinf Plast Compos* 2022; 41(15–16): 602–623.
25. Tran T. A study on nested two-tube structures subjected to lateral crushing. *Thin-Walled Struct* 2018; 129: 418–428.
26. Dauphin Y, Brunelle A, Medjoubi K, et al. The prismatic layer of Pinna: a showcase of methodological problems and preconceived hypotheses. *Minerals* 2018; 8(9): 22–28.
27. Erdin ME, Baykasoglu C and Cetin MT. Quasi-static axial crushing behavior of thin-walled circular aluminum tubes with functionally graded thickness. *Procedia Eng* 2016; 149: 559–565.
28. Cai Z, Deng X and Wang G. Energy absorption analysis under in-plane impact of hexachiral honeycomb with different arrangements. *Arch Civ Mech Eng* 2024; 24(2): 77.
29. Wang G, Cai Z and Deng X. In-plane dynamic impact mechanical properties of novel bi-directional hierarchical honeycomb. *Eng Fract Mech* 2024; 300: 110009.
30. Hou S, Li Q, Long S, et al. Crashworthiness design for foam filled thin-wall structures. *Mater Des* 2009; 30(6): 2024–2032.
31. Wang G, Liu F and Deng X. In-plane mechanical behavior design of triangular gradient rib honeycombs. *Thin-Walled Struct* 2024; 205: 112415.